Research Article | Vol. 29, No. 7 / 29 March 2021 / Optics Express 10434
Optics EXPRESS

Effects of optical activity to Mueller matrix ellipsometry of composed waveplates

DANIEL VALA,[1,2,3,6] PIERRE KOLEJÁK,[1,2,4] KAMIL POSTAVA,[1,2,7] MORTEN KILDEMO,[3] PAVLÍNA PROVAZNÍKOVÁ,[5] AND JAROMÍR PIŠTORA[1]

[1]*IT4Innovations, National Supercomputing Center, VšB – Technical University of Ostrava, 17. listopadu 15, 708 00 Ostrava-Poruba, Czech Republic*
[2]*Faculty of Materials Science and Technology, VšB – Technical University of Ostrava, 17. listopadu 15, 708 33 Ostrava-Poruba, Czech Republic*
[3]*Department of Physics, NTNU Norwegian University of Science and Technology, NO-7491 Trondheim, Norway*
[4]*Institute of Electronics, Microelectronics and Nanotechnology, UMR 8520 CNRS, Cité Scientifique, Avenue Henri Poincaré CS 60069, 59 652 Villeneuve d'Ascq Cedex, France*
[5]*Meopta - Optika, s.r.o., Kabelíkova 1, 750 02 Přerov, Czech Republic*
[6]*daniel.vala@vsb.cz*
[7]*kamil.postava@vsb.cz*

Abstract: Mueller matrix ellipsometry has been used to precisely characterize quartz waveplates for demanding applications in the semiconductor industry and high precision polarimetry. We have found this experimental technique to be beneficial to use because it enables us to obtain absolute and precise measurement of retardation in a wide spectral range, waveplate orientation, and compound waveplate adjustment. In this paper, the necessity of including the optical activity in the Mueller matrix model and data treatment is demonstrated. Particularly, the optical activity of the quartz influences the adjustment of misalignment between the perpendicularly oriented waveplates of the compound biplate. We demonstrate that omitting the optical activity from the model leads to inaccurate values of the misalignment. In addition, the depolarization effects caused by a finite monochromator bandwidth is included in the model. Incorporation of the optical activity to the Mueller matrix model has required a development of rigorous theory based on appropriate constitutive equations. The generalized Yeh's matrix algebra to bianisotropic media has been used for the calculation of the eigenmodes propagation in chiral materials with reduced symmetry. Based on the applied method, the authors have proposed approximated analytical form of the Mueller matrix representing optically active waveplate and biplate and provided discussion on the analytical and numerical limits of the method.

1. Introduction

Waveplates are polarization optical components with a broad field of applicability across the semiconductor industry [1,2], quality inspection in manufacturing processes [3,4], THz spectroscopy [5,6], analytical chemistry [7–9] and polarimetry [10–13]. From a polarimetric point of view, the waveplates are commonly used in optical spectrometers as compensators [14]. It is no exception to use the waveplates during high-precision-demanding procedures like calibration of various custom experimental setups [15–18]. Then, the quality of the used waveplates directly affects the quality of acquired data [19–24] and above mentioned industrial technological properties.

Typically, industrial inspection of manufactured waveplates is based on a configuration with two crossed polarizers and the waveplate being placed between them [25]. The method determines the orientation of the waveplate fast-axis and its single-wavelength relative retardation. The

#418186 https://doi.org/10.1364/OE.418186
Journal © 2021 Received 22 Dec 2020; revised 14 Feb 2021; accepted 23 Feb 2021; published 18 Mar 2021

Optics EXPRESS

waveplate retardation is given as the difference between phases of two orthogonal linearly polarized eigenmodes propagating through the plate [26,27]. Waveplates of higher order exhibit high chromatic dispersion, however, broadly used zero-order waveplate would be undesirably thin. To overcome this inconvenience, the waveplates are composed by two thicker higher order plates with crossed optical axes [28], so called biplates. However, this method may be insufficient nowadays, as the users demands on the waveplates precision fabrication raises significantly. Therefore, precise characterization of the composed waveplates in order to obtain the parameters of each of the constituting waveplate can be challenging, and proper treatment has to be established as various non-trivial effects may come to raise.

In our previous paper [29] we have shown the advantage of complete Mueller matrix inspection and we have demonstrated that spectral characterization and industrial inspection of waveplates requires the inclusion of the depolarization effects [30–32]. The Mueller calculus and Mueller matrix spectroscopic ellipsometry is a particularly advantageous [10] method for proper waveplate analysis as it is spectroscopic, non-destructive, and capable of incorporating all the mentioned phenomena due to high experimental precision [33,34]. In Ref. [29] we have also shown the presence of the nonzero circular birefringence related to optical activity (OA) using the Lu-Chipman decomposition [35] of the quartz waveplates experimental data.

In this article, the Mueller matrix spectroscopic ellipsometry in transmission configuration is used for precise quartz single waveplate and quartz waveplate biplates characterization. We exclusively measure the waveplates aligned with the optical axis perpendicular to the propagation direction and we demonstrate, that the effect of the OA can not be neglected to process the experimental data correctly. In studies [36,37], Mueller matrix ellipsometry was applied to study waveplate multiplets. Its model simplicity has an advantage in the calibration procedures involving the waveplates including their misalignment error. As long as the method doesn't account for the OA dispersion in the waveplates, the net elliptical properties of the waveplate effectively project into other waveplate characteristics causing their quasi-oscillatory behaviour. Therefore, we derived a rigorous model of the Mueller matrix including the gyration effects from the theory based on Fedorov's [38,39] and Yeh's [40] work and the Condon-Fedorov's constitution relations [38,41]. The rigorous model including the OA is compared to the experimental data for single waveplates and biplates. We further show, that the OA effect is separable and independent of other waveplate (biplates) characteristics like plates misalignment. All those parameters are obtained with very high numerical precision and great fit stability.

The paper is structured as follows: In Sec. 2, the rigorous Mueller matrix models for optically active single waveplates and waveplate biplates are derived. Section 3 describes the biplate samples and experimental configuration. Measurement analysis is divided into two steps. First of all, we model the parameters of single waveplates to use them during the biplate analysis afterwards in order to obtain precise biplate parameters including their misalignment. To demonstrate the necessity of using a Mueller matrix model with OA, we compare the experimental data with the models with and without OA. To understand the OA contribution in the Mueller matrix, in Appendix A., we generalize the standard Yeh's matrix algebra to bianisotropic and optically active media using various constitutive relation formalism, and in particular, eigenmodes for uniaxial chiral media are calculated in Appendix B.. Detailed derivation of the proposed Mueller matrix form is given in Appendix C.. In Appendix D., we offer an algebraic analysis on the manifestation difference between the misalignment and the OA in the proposed Mueller matrices.

2. Mueller matrices of waveplates including optical activity

Mueller matrix represents the complete polarimetric information, which can be acquired from the interaction between the sample and the polarized light, including depolarizations.

Optics EXPRESS

2.1. Mueller matrix of a standard linear retarder

The reduced 4×4 Mueller matrix (all elements are divided by M_{11}) describing a single waveplate consisting of a uniaxial anisotropic material with the optical axis parallel to the waveplate surface at the normal incidence (linear retarder) is given [14] as

$$\mathbf{M}_{\mathrm{R,LIN}}(\varphi,\,\Gamma) = \begin{bmatrix} 1 & 0 & 0 & 0 \\ 0 & \cos^2 2\varphi + \cos\Gamma \sin^2 2\varphi & (1-\cos\Gamma)\sin 2\varphi \cos 2\varphi & -\sin 2\varphi \sin\Gamma \\ 0 & (1-\cos\Gamma)\sin 2\varphi \cos 2\varphi & \sin^2 2\varphi + \cos\Gamma \cos^2 2\varphi & \cos 2\varphi \sin\Gamma \\ 0 & \sin 2\varphi \sin\Gamma & -\cos 2\varphi \sin\Gamma & \cos\Gamma \end{bmatrix}, \tag{1}$$

where φ is the azimuthal angle between the waveplate fast-axis and the vertical laboratory coordinate, and

$$\Gamma(\lambda) = \frac{2\pi}{\lambda}\left[n_{\mathrm{f}}(\lambda) - n_{\mathrm{s}}(\lambda)\right] d, \tag{2}$$

is the retardation angle between the fast and slow eigenmodes propagating in the waveplate with the refractive indices $n_{\mathrm{f,s}}$, which is dependent on the wavelength λ and the waveplate thickness d. Normally, the fast and slow eigenmodes correspond to linearly polarized eigenmodes propagating with ordinary and extraordinary refractive indices $n_{\mathrm{e,o}}$, respectively.

2.2. Mueller matrix of a single waveplate with optical activity

Natural or synthetic quartz monocrystal is very common material for the waveplate manufacturing. It belongs to uniaxial trigonal crystal symmetry [42,43] (Hermann-Maugin 32 point group) and is therefore optically active [44–46]. Across the literature, the effect of the OA in quartz (or quartz waveplates) has been studied in the configuration with the quartz optical axis being parallel (z-cut) to the direction of propagation [47] so far. Usually, the effect of the OA with optical axis perpendicular to the propagation direction is said to be experimentally negligible [48], which is inadequate for waveplate precise quality and properties control.

In our preceding work [29], the presence of non-zero circular birefringence was discovered using Lu-Chipman decomposition of experimental Mueller matrix, which we interpreted as the presence of the OA. Rigorous incorporation of the OA in waveplates requires (i) a solution of Maxwell equations based on a proper set of material equations introducing the gyration tensors $\hat{\alpha}$ and $\hat{g}$ with respect to the 32 point group which leads to the wave equation of the problem. Definition of the constitutive equations and a detailed discussion of suitability of various approaches is given in Appendix A., (ii) calculation of generally elliptical eigenmodes propagating in the waveplate based on the wave equation evaluation (see Appendix B.), (iii) derivation of Mueller matrix including the OA as a function of the chirality parameter

$$\kappa = \frac{1}{2G}\left[\left(n_{\mathrm{e}}^2 - n_{\mathrm{o}}^2\right) - \sqrt{\left(n_{\mathrm{e}}^2 - n_{\mathrm{o}}^2\right)^2 + 4G^2}\right], \tag{3}$$

where the spectrally dependent scalar gyration parameter G for our configuration is given by the gyration tensor component g_{11} derived in [47],

$$G = g_{11} = \frac{A_1 \lambda^3}{\left(\lambda^2 - B_1^2\right)^2}. \tag{4}$$

In this Section, we show the model of the Mueller matrix including the OA effect from the Jones matrix of an elliptical retarder, see Appendix C., Eq. (33). Eigenmodes propagating through a medium described by Eq. (33) are ellipticaly polarized and are propagating with corresponding

Optics EXPRESS

refractive indices. Since the effect of the OA is very small, the elliptical eigenmodes can be approximated as linear-like eigenmodes. Therefore, it is justifiable to linearly approximate κ, as long as it is a function of eigenmodes ellipticity, see Appendix C., Eq. (34). Moreover, the indices of refraction of the linear-like eigenmodes become equal with high precision to ordinary and extraordinary indices of refraction, respectively, see Appendix C., Eq. (31). The Mueller matrix of an elliptic retarder $\mathbf{M}_{\mathrm{R,EL}}(\varphi,\,\Gamma,\,\kappa)$ is in the linear approximation in the form

$$\mathbf{M}_{\mathrm{R,EL}}(\varphi,\,\Gamma,\,\kappa) = \mathbf{M}_{\mathrm{R,LIN}}(\varphi,\,\Gamma) + \mathbf{\Delta M}_{\mathrm{OA}}(\varphi,\,\Gamma,\,\kappa)\,, \tag{5}$$

where

$$\mathbf{\Delta M}_{\mathrm{OA}}(\varphi,\,\Gamma,\,\kappa) = \begin{bmatrix} 0 & 0 & 0 & 0 \\ 0 & 0 & 2\kappa\sin\Gamma & 4\kappa\cos 2\varphi\sin^2\frac{\Gamma}{2} \\ 0 & -2\kappa\sin\Gamma & 0 & 4\kappa\sin 2\varphi\sin^2\frac{\Gamma}{2} \\ 0 & 4\kappa\cos 2\varphi\sin^2\frac{\Gamma}{2} & 4\kappa\sin 2\varphi\sin^2\frac{\Gamma}{2} & 0 \end{bmatrix}, \tag{6}$$

is the matrix describing the effect of the OA by introducing linearly approximated chirality parameter κ.

In our approximation, we treat the quantity κ as a real parameter. This is in a conformity with the usual quartz waveplates application range over its transparent region. The Jones matrix (33) is valid generally for any of the parameter being complex, in contrast with the Mueller matrix (5). This is due to the form (Kronecker product) of the transformation Eq. (36). Therefore, in the vicinity of absorption bands, the Eq. (5) must be calculated assuming complex κ. The measurements over this spectral region is out of the scope of the paper and will not be further elaborated.

The experimental validity condition of the linear approximation is obtained by analyzing the quadratic (erroneous) terms in the Taylor series of $\mathbf{\Delta M}_{\mathrm{OA}}$ focused on the maximal possible error. The criterion is then set to $8\kappa^2<\sigma$, where σ stands for an error of the experimental Mueller matrix elements. Note, that in our experimental configuration, $\sigma = 0.001$ implies the condition for $\kappa<0.0112$. This criterion is fulfilled for the quartz waveplates [47] in the spectral range of further shown experiments.

The non-approximated matrix $\mathbf{M}_{\mathrm{R,EL}}$ stands for an equivalent solution with Mueller matrices of an elliptical retarder presented in [49] [Eq. (22)], in Ref. [50] [Eq. (14)] or on page 289 in Ref. [51]. Our proposed solution applied to the subject discussed in this paper provides the opportunity to have deeper physical insight into the problematic and to get more intuitive way of the result interpretation and discussion, as we show later. Also, in contrast with Eq. (22) in Ref. [49], we reduce the number of needed fitting parameters.

2.3. Mueller matrix of a biplate

The Mueller matrix for a biplate given by the product of Mueller matrices $\mathbf{M}_{\mathrm{R,EL1}}$, $\mathbf{M}_{\mathrm{R,EL2}}$ each representing a standalone waveplate with its own retardation Γ_1, Γ_2, respectively, and azimuthal angle φ_1, φ_2, respectively, is in the form

$$\mathbf{M}_{\mathrm{R,WB}} = \mathbf{M}_{\mathrm{R,EL2}}(\varphi_2,\,\Gamma_2,\,\kappa)\,\mathbf{M}_{\mathrm{R,EL1}}(\varphi_1,\,\Gamma_1,\,\kappa)\,. \tag{7}$$

Each waveplate is manufactured from the same material, therefore we assume the same optical activity dispersion, $\kappa_1 = \kappa_2 = \kappa$.

Note, that from now on, we will focus on the 3×3 Mueller submatrix $M_{22}\ldots M_{44}$ only, due to the structure of (1) and above discussed Mueller matrices.

Optics EXPRESS

3. Measurements and data processing

We applied spectral ellipsometric measurements using the dual rotating compensator Mueller matrix ellipsometer RC2-DI from Woollam company, which measures a full Mueller matrix in the spectral range from 0.74 to 6.42 eV (wavelength ranging from 193 to 1700 nm). The waveplates are measured in the normal-incidence transmission geometry.

We have investigated biplates consisting of a stack of two c-cut right-handed synthetic α-quartz high-order waveplates belonging to the 32 point group. The biplate constituting waveplates are attached to each other, having its fast axes mutually perpendicular, by perfectly polished surfaces, and therefore hold together only by the presence of Van der Waals forces. This fact allows us to split the biplate without causing damage, and measure each waveplate of the biplate separately to obtain its accurate parameters (thicknesses, retardation angles).

3.1. Single waveplate measurements

The measurements of both single waveplates constituting the biplate were performed in the normal incident transmission configuration for all azimuthal angles from 0° to 360° by the angle step of 5°. Figure 1 shows typical spectra (black curves) of the Mueller 3×3 submatrix for the high-order single waveplate. The oscillations correspond to the spectrally dependent wavelength retardation. The waveplate order m (e.g. $m = 9$ for $\lambda = 500$ nm) determines the oscillations density, which gets denser with increasing photon energy, while the oscillations amplitude decreases. The decreasing amplitude modulation for high photon energy is due to the dense oscillations spectral averaging caused by a finite monochromator bandwidth [52,53]. In our case, this corresponds to the spectral resolution of dispersion grating and finite pixel size of the CCD detector. The attenuation compensation is based on the incoherent summation of Mueller matrix model, which is commented in our preceding work (Eqs. (3) and (4) in [29]) in the detail. The spectral step we use in the averaging function is $\delta\lambda = 1.075$ nm.

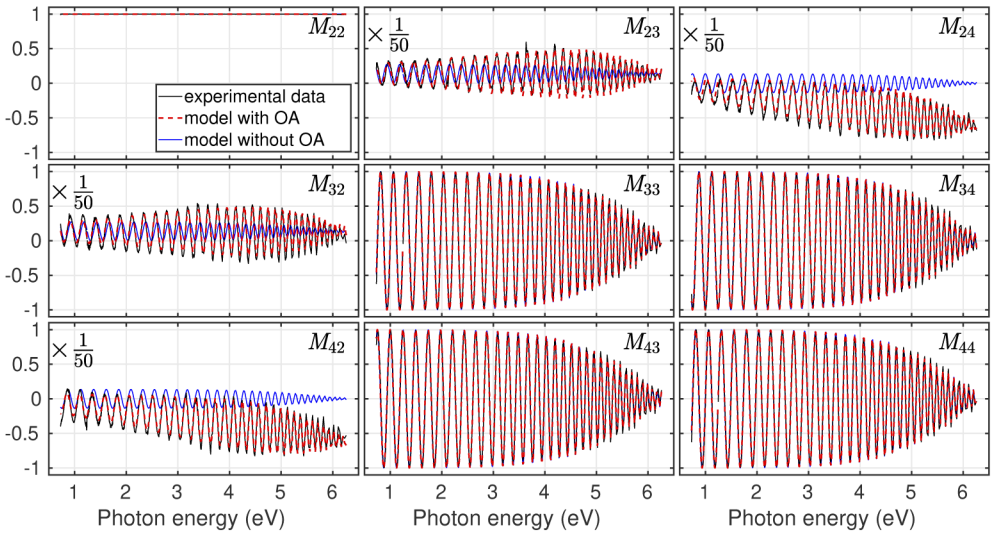

Fig. 1. Mueller 3×3 submatrix of the single waveplate of thickness $d_1 = 536.63\,\mu$m at the azimuthal angle $\varphi_1 = 180.078°$. The data are compared to the model of standard linear retarder (without the effect of OA) and to the model including the OA effect. Model with the OA effect disregarded is not capable to properly describe both the dispersion and the attenuation exhibiting in the first row and the first column of the Mueller submatrix off-diagonal elements. Note, that the axes of those Mueller matrix elements are scaled by the factor of $1/50$.

Optics EXPRESS

The data are compared to the model (1) including spectral averaging (blue curve) over high energy spectral range and shows a relatively good fit of the Mueller matrix elements M_{33}, M_{34}, M_{43}, M_{44}. For azimuthal rotations, for which the waveplate has its axes nearly perfectly aligned with the laboratory coordinate system, the oscillation amplitude within the measured elements M_{23}, M_{24}, M_{32}, M_{42} decreases with decreasing photon energy over low energy spectral ranges. Together with the modulation of the oscillations dispersion within these elements, it corresponds to the effect of the optical activity dispersion in the quartz waveplate. To properly fit all the elements of the Mueller submatrix, we model the influence of OA (red curve) using (5) with the spectral averaging included. The parameters $A_1 = 0.0277$ nm, $B_1 = 105.6$ nm of (4) are taken from Ref. [47]. The fitted thicknesses for each waveplate are $d_1 = 536.63$ μm, $d_2 = 549.03$ μm, and absolute retardations were obtained. The dispersion of n_o, n_e are taken from Ref. [54,55]. Note, the OA effects are very small in comparison with the linear retardation, therefore M_{23}, M_{24}, M_{32}, M_{42} Mueller matrix elements are expanded 50 times. Despite the fine effect of the OA, the response in the measured Mueller matrix is well detectable and shows high sensitivity of the proposed method.

3.2. *Fine control of waveplate biplate misalignment*

Biplate consists of two high-order waveplates with crossed optical axes to produce an effective low-order waveplate. Possible imperfections during the biplates manufacturing can introduce a misalignment between the waveplates, as they may not be aligned to each other with their optical axes being perfectly perpendicular, see Fig. 2. The misalignment between the waveplates is then defined as

$$\Phi = \varphi_1 - \varphi_2 - 90^\circ. \tag{8}$$

We have shown [29], that Mueller matrix approach is significantly sensitive to the waveplate misalignment. In this Section, we propose a robust and sensitive inspection method for the biplate misalignment determination based on a rigorous Mueller matrix model including OA.

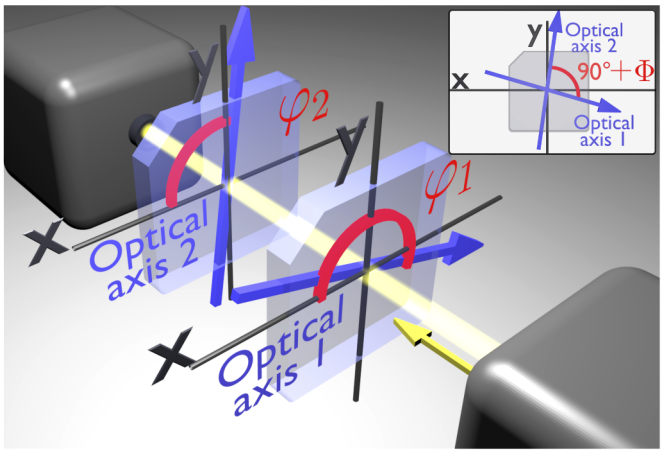

Fig. 2. Schematic configuration of the waveplates constituting the biplate. Their optical axes are ideally perpendicular, $\varphi_1 - \varphi_2 = 90^\circ$. The manufacture inaccuracy causes the deviation from this perpendicularity, and introduces the missalignment Φ, as shows the inset figure.

To simulate the misalignment between the waveplates of the biplate, one waveplate was placed fixed to the ellipsometer sample holder, while the second waveplate was rotated around the relative angle of 90° between the waveplates.

Optics EXPRESS

Figure 3 shows the Mueller submatrix spectra of the biplate with controlled φ_1 (and therefore controlled Φ) ranging from 185.7° to 186.1° with step 0.1° (Φ is ranging from −0.2° to 0.2° with step 0.1°). The Mueller 3 × 3 submatrix (right part of the Fig. 3) shows the dominant effect of the linear retardation dispersion without the dense spectral oscillations, which are typical for high-order waveplates. The presence of minor oscillations corresponds to combination of the misalignment between waveplates of the biplate and its optical activity. Left part of Fig. 3 shows the detail of the Mueller submatrix first column. Each curve of the same color corresponds to different φ_1, and therefore to different misalignment. First, the data are compared to the Mueller matrix model of the cascade of two standard linear retarders (7) without including the OA (blue lines), $\kappa = 0$, which is insufficient for the proper analysis of the misalignment between two waveplates. In contrast, the model (7) including the OA (red lines), $\kappa \neq 0$, shows very good fit of the measured data. The slight mismatch from the data is just above experimental error of the Mueller matrix elements (0.001). At this scale, the errors are inevitable. They could origin in the calibration quality, systematic errors, non-ideal plates parallelity, waveplate miscut or precision of used material dispersion parameters. The parameters $A_1 = 0.0277$ nm, $B_1 = 105.6$ nm of (4) are taken from Ref. [47], and the waveplate thicknesses ($d_1 = 536.63\ \mu$m, $d_2 = 549.03\ \mu$m), and retardation dispersions were determined from the measurements of each of the separated waveplates. The fitted parameters φ_1 and φ_2 were obtained from the fit of each biplate measurement independently. The Fig. 4 shows the waveplate misalignment obtained for the data fitted to Eq. (8) point by point. The fitted values of φ_1, φ_2 and Φ corresponding to each curve in Fig. 3 are shown in Table 1.

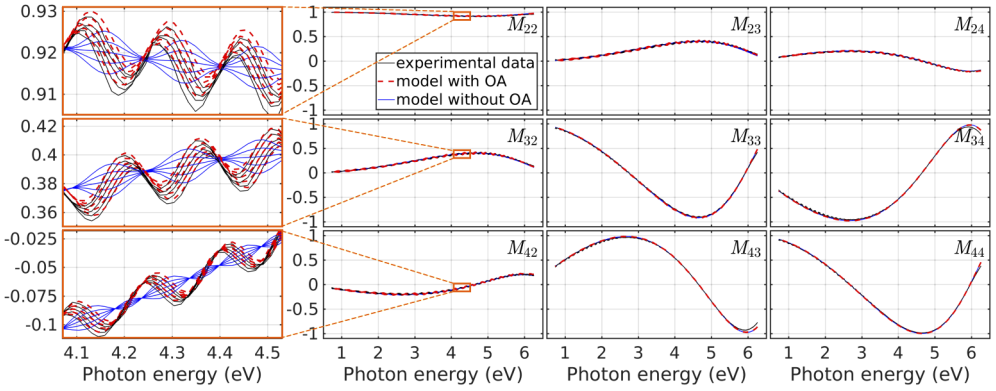

Fig. 3. Experimental Mueller submatrix for biplate. Each curve of the same color represents different value of φ_1 ranging from 185.7° to 186.1° with step 0.1°. Comparison between data and models with and without the effect of the OA shows the significance of the the OA phenomenon in proper determination of the misalignment, which is exhibited by the presence of the minor oscillation shown in the detail of the submatrix first column. Note, that the energy range from 4.1 eV to 4.5 eV corresponds to the wavelength range from 302.4 nm to 275.5 nm.

Table 1. Fitted values of φ_1, φ_2 and Φ for representative Mueller submatrix spectra shown in Fig. 3.

φ_1 (degree)	185.711	185.812	185.912	186.015	186.116
φ_2 (degree)	95.930	95.931	95.932	95.934	95.936
Φ (degree)	−0.218	−0.119	0.019	0.080	0.179

Figure 4(b) demonstrates the misalignment fit stability. Each point was calculated as a subtraction of the misalignment from consequent values during one waveplate azimuthal rotation.

Optics EXPRESS

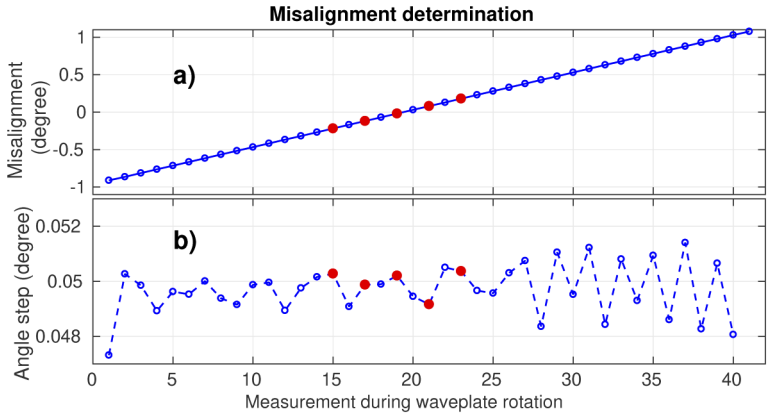

Fig. 4. a) Fitted values of the misalignment for each measurement with various azimuthal rotations of the waveplates. b) Fit stability of the misalignment determination is demonstrated comparing the calculated angle steps to the nominal value of 0.05°. Red points correspond to selected measurements presented in Fig. 3.

The mean value of the angle step corresponds well with the actual experimental angle step of 0.05°, which shows high stability of the misalignment determination without any correlation to the optical activity. Red points demonstrate selected measurements presented in Fig. 3.

Ultimately, it is important to mention, that excluding the presence of the OA from the model is leading to the misinterpretation of the OA with incorrect misalignment values. We show the linear expansion of the Mueller matrix of biplate (7) for both the misalignment (Φ) and the OA (κ) in Appendix D. to understand the significant difference between oscillations induced by κ and Φ. Both misalignment (45) and OA (46) dispersions have similar behavior in the form of minor oscillations shown in Fig. 3. These oscillations origin in the high-density trigonometric terms including only the retardation Γ_1 or Γ_2. If one tries to fit the data using the model without the OA (demonstrated for our case), the misalignment of around 0.5° will tend to compensate the OA with its amplitude. Nonetheless, such model does not match the data over the whole spectral range, because κ has spectral dependence given by Eq. (4), and thus, the amplitude of the oscillations changes. Such model without the OA also results in erroneous waveplate thicknesses, because the terms of $\mathbf{m}_\kappa$ and $\mathbf{m}_\Phi$ matrices are defined by terms in cosines or sines of the waveplates retardation. It is curious, that sine terms of one matrix correspond to appropriate cosine terms of second matrix and vice versa. Therefore, the fit without the OA will result in thicknesses imperfections for both waveplates by 6.4 μm to compensate the phase shift. However, their thickness difference remains the same due to the major influence of the linear retarder (1). It results in the fact, that low-density trigonometric terms of the retardation difference $\Gamma_1 - \Gamma_2$ are not able to be compensated and thus make significant difference in the spectrum. Nevertheless, the sine and cosine terms are not only shifted one from another, but they also represent different functions which do not match the data, especially if both misalignment and the OA influence are present.

4. Conclusion

In this article, biplates represented by a couple of high-order waveplates with crossed optical axes have been measured by means of Mueller matrix ellipsometry in the spectral range from 193 to 1700 nm. In order to obtain accurate values of biplate parameters including the biplate misalignment, we theoretically revealed and experimentally confirmed, that it is necessary to include the effects of the optical activity into the derived model of Mueller matrix. To obtain the

Optics EXPRESS

exact solution of the Mueller matrix, it is needed to find the eigenmodes and propagation constants of the optically active medium represented by the quartz waveplate in this case. We emphasize, that omitting the optical activity from the model would lead to the incorrect interpretation of the optical activity phenomenon with the inaccurate values of the waveplate misalignment.

We believe, that the proposed method, which has an advantage in its great experimental sensitivity, fit stability and repeatability, could stand as a fast non-destructive industrial analysis for the accurate in-situ control of the biplates misalignment during the manufacturing process. Moreover, the concept based on the rigorous model can be extended for the analysis of the waveplate multiplets. In addition, waveplates parameters obtained from precise Mueller matrix characterization can be further used for the accuracy improvement of calibration procedures of various experimental setups involving waveplates and Mueller calculus based calibration procedures.

A. Wave equation in chiral media

A.1. Covariant form of Maxwell equations

In the following, the plane monochromatic wave is described by the electric field in the form

$$\mathbf{E} = \mathbf{E}_0\, e^{i(\omega t - \mathbf{k}\cdot\mathbf{r})}, \tag{9}$$

where ω is the angular frequency and $\mathbf{k}$ is the wave vector related to the refraction vector $\mathbf{N}$ using the wave number in a vacuum $k_0 = \omega/c$, where c is the light speed in a vacuum, as

$$\mathbf{k} = k_0\mathbf{N}. \tag{10}$$

The curl Maxwell equations for the monochromatic plane waves (9) relating the electric and magnetic fields $\mathbf{E}_0$, $\mathbf{H}_0$ to its displacements $\mathbf{D}_0$, $\mathbf{B}_0$, respectively, can be written in the covariant form

$$\mathbf{N}^{\times}\mathbf{E}_0 = c\mathbf{B}_0, \tag{11a}$$

$$\mathbf{N}^{\times}\mathbf{H}_0 = -c\mathbf{D}_0, \tag{11b}$$

$$c = \frac{1}{\sqrt{\varepsilon_0\mu_0}}, \tag{11c}$$

where ε_0 and μ_0 are the permittivity and permeability in a vacuum, respectively, and

$$\mathbf{N}^{\times} = \begin{bmatrix} N_x \\ N_y \\ N_z \end{bmatrix}^{\times} \equiv \begin{bmatrix} 0 & -N_z & N_y \\ N_z & 0 & -N_x \\ -N_y & N_x & 0 \end{bmatrix} = \frac{1}{k_0}\begin{bmatrix} 0 & -k_z & k_y \\ k_z & 0 & -k_x \\ -k_y & k_x & 0 \end{bmatrix}. \tag{12}$$

The direction of wave propagation is given by the wave vector $\mathbf{k} = k_0 \left[N_x\ N_y\ N_z\right]^{\mathrm{T}}$, and a set of constitutive relations must be chosen.

For a general anisotropic gyrotropic (bianisotropic) and magnetic media, various forms of constitutive equations have been developed [56] and compared to each other [57,58]. Nowdays, Tellegen [59] and Condon-Fedorov [38,41] material equations seem to be the most convenient and acceptable form of constitutive relations.

Optics EXPRESS

A.2. Tellegen constitutive relations

Tellegen relations take the form

$$\mathbf{D}_0 = \hat{\varepsilon}\mathbf{E}_0 + \hat{\xi}\mathbf{H}_0, \tag{13a}$$

$$\mathbf{B}_0 = \hat{\mu}\mathbf{H}_0 + \hat{\zeta}\mathbf{E}_0\,. \tag{13b}$$

The material tensors are in the form

$$\hat{\varepsilon} = \varepsilon_0\hat{\varepsilon}_\mathrm{r}, \tag{14a}$$

$$\hat{\mu} = \mu_0\hat{\mu}_\mathrm{r}, \tag{14b}$$

where $\hat{\varepsilon}_\mathrm{r}$, $\hat{\mu}_\mathrm{r}$ are the relative permittivity and the relative permeability tensors, respectively, and $\hat{\xi}$, $\hat{\zeta}$ are general second-rank coupling tensors, where we use the convention [60]

$$\hat{\xi} = (\hat{\nu} + i\hat{\eta})\sqrt{\varepsilon_0\mu_0}, \tag{15a}$$

$$\hat{\zeta} = \left(\hat{\nu} - i\hat{\eta}^\mathrm{T}\right)\sqrt{\varepsilon_0\mu_0}. \tag{15b}$$

Parameter $\hat{\nu}$ is related with the reciprocity of the medium, while $\hat{\eta}$ describes the optical activity. Substituting (13) into (11) and eliminating $\mathbf{H}_0$, the wave equation for $\mathbf{E}_0$ in the most general form is obtained:

$$\left[c^2\hat{\varepsilon} + \mathbf{N}^\times\hat{\mu}^{-1}\,\mathbf{N}^\times + c\left(\hat{\xi}\hat{\mu}^{-1}\mathbf{N}^\times - \mathbf{N}^\times\hat{\mu}^{-1}\hat{\zeta}\right) - c^2\hat{\xi}\mu^{-1}\hat{\zeta}\right]\mathbf{E}_0 = 0, \tag{16}$$

which represents a matrix form of the wave equation and can be implemented in the standard Yeh's matrix formalism to calculate reflection, transmission and wave-guided phenomena of multilayered structure.

A.3. Condon-Fedorov constitutive relations

For reciprocal chiral media ($\hat{\nu} = 0$, $\hat{\eta} \neq 0$) a set of Condon-Fedorov constitutive relations is commonly used:

$$\mathbf{D}_0 = \hat{\varepsilon}\mathbf{E}_0 + \frac{1}{c}i\hat{\alpha}\mathbf{H}_0, \tag{17a}$$

$$\mathbf{B}_0 = \hat{\mu}\mathbf{H}_0 + \frac{1}{c}i\hat{\beta}\mathbf{E}_0, \tag{17b}$$

where the tensors $\hat{\alpha}$ and $\hat{\beta}$ are the second-rank tensors describing the effect of optical activity. Applying the Onsager-Casimir principle [61–63] on Eq. (17) [64], the Condon-Fedorov equations can be rewritten [65] in the commonly used form as

$$\mathbf{D}_0 = \hat{\varepsilon}\mathbf{E}_0 + \frac{1}{c}i\hat{\alpha}\mathbf{H}_0, \tag{18a}$$

$$\mathbf{B}_0 = \hat{\mu}\mathbf{H}_0 - \frac{1}{c}i\hat{\alpha}^\mathrm{T}\mathbf{E}_0, \tag{18b}$$

where $\hat{\alpha}$ is the optical activity pseudotensor [48,57]. Using the same procedure as previously and using (11c), the equivalent wave equation is derived [48,66]:

$$\left[\hat{\varepsilon}_\mathrm{r} + \mathbf{N}^\times\hat{\mu}_\mathrm{r}^{-1}\,\mathbf{N}^\times + i\left(\hat{\alpha}\hat{\mu}_\mathrm{r}^{-1}\mathbf{N}^\times + \mathbf{N}^\times\hat{\mu}_\mathrm{r}^{-1}\hat{\alpha}^\mathrm{T}\right) - \hat{\alpha}\hat{\mu}_\mathrm{r}^{-1}\hat{\alpha}^\mathrm{T}\right]\mathbf{E}_0 = 0, \tag{19}$$

and following tensor identity is valid [38]:

$$\hat{\alpha}\hat{\mu}_\mathrm{r}^{-1}\mathbf{N}^\times + \mathbf{N}^\times\hat{\mu}_\mathrm{r}^{-1}\hat{\alpha}^\mathrm{T} \equiv (\hat{g}\,\mathbf{N})^\times\,. \tag{20}$$

The wave equation is then in the form

$$\left[\hat{\varepsilon}_\mathrm{r} + \mathbf{N}^\times\hat{\mu}_\mathrm{r}^{-1}\,\mathbf{N}^\times + i\,(\hat{g}\,\mathbf{N})^\times\right]\mathbf{E}_0 = 0. \tag{21}$$

Special case for bi-gyrotropic media was described in Ref. [67].

Optics EXPRESS

A.4. Born-Landau constitutive equations

Equation (20) stands for a definition of the gyration tensor $\hat{g} = g_{ij}$, which describes the optical activity effect in Born-Landau [68] constitutive relations

$$\mathbf{D}_0 = \hat{\varepsilon}\mathbf{E}_0 + i\varepsilon_0\mathbf{G}\times\mathbf{E}_0 = \left(\hat{\varepsilon} + i\varepsilon_0\mathbf{G}^{\times}\right)\mathbf{E}_0, \tag{22a}$$

$$\mathbf{B}_0 = \hat{\mu}\,\mathbf{H}_0\,, \tag{22b}$$

where $\mathbf{G} = \hat{g}\mathbf{N}$ is the gyration vector related with scalar gyration parameters

$$G = g_{ij}l_il_j = g_{11}l_1^2 + g_{22}l_2^2 + g_{33}l_3^2 + (g_{12}+g_{21})\,l_1l_2 + (g_{13}+g_{31})\,l_1l_3 + (g_{23}+g_{32})\,l_2l_3, \tag{23}$$

and l_i, l_j are directional cosines of the wave normal with respect to the coordinate system given by a triad of unit vectors c_i,

$$l_i \equiv \cos\left(\measuredangle N_i\, c_i\right). \tag{24}$$

A.5. Relation between the constitutive equations for optically active media

By the comparison of (15) with (18) we can see, that Condon-Fedorov equations are a special case of Tellegen material relations for *reciprocal chiral* media:

$$\hat{\xi} = \frac{1}{c}i\hat{\eta} \leftrightarrow \frac{1}{c}i\hat{\alpha}, \tag{25a}$$

$$\hat{\zeta} = -\frac{1}{c}i\hat{\eta}^{\mathrm{T}} \leftrightarrow -\frac{1}{c}i\hat{\alpha}^{\mathrm{T}}. \tag{25b}$$

Here, we justly state, that Condon-Fedorov and Born-Landau approaches are not fully equivalent. We strongly recommend the kind reader to see the detailed discussion in Ref. [69]. However, for our particular case of transparent waveplates, both constitutive equations can be applied. Moreover, within our (and generally achievable) experimental precision, the difference is negligible and these two approaches can be used in the equivalent way providing the same results for any, even absorbing material [69].

B. Eigenmodes propagating in chiral uniaxial media of point group 32

The manifestation of the OA for light propagation along the optical axis of nonmagnetic uniaxial gyrotropic media of 32 point group (i.e. quartz) is well-known fact. We emphasize, that the OA effect in quartz is given intrinsically because of its non-centrosymmetricity. Also, the OA has similar size along the principal axes of $\hat{\alpha}$ (or $\hat{g}$) [47], and is therefore non-negligible within the precision of contemporary Mueller matrix ellipsometry. Concluding, the OA is present in all possible experimental configurations (or cuts) of the quartz plate including light propagation perpendicular to the optical axis. In the following, we will discuss two important special orientations of the crystal optical axis.

For the propagation along the optical axis, the material tensors in (19) reduce to $\hat{\varepsilon}_{\mathrm{r}} = \mathrm{diag}\,[\varepsilon_{11}\ \varepsilon_{11}\ \varepsilon_{33}]$, $\hat{\mu}_{\mathrm{r}} = \mathrm{diag}\,[1\ 1\ 1]$, and $\hat{\alpha} = \mathrm{diag}\,[\alpha_{11}\ \alpha_{11}\ \alpha_{33}]$. Assuming normal incidence only, $\mathbf{N} = [0\ 0\ N_z]^{\mathrm{T}}$. The refractive indices of corresponding circularly polarized eigenmodes $N_{z,\alpha,k=\{1,2,3,4\},\parallel}$ have been published several times [48,57,66], and take the form

$$N_{z,\alpha,k,\parallel} = \pm\sqrt{\varepsilon}_{11} \pm \alpha_{11}\,. \tag{26}$$

Propagation perpendicular to the optical axis is carried out introducing the rotation tensor of the Cartesian coordinate system $\mathbf{R}$, which is defined by a triad of Euler angles defined same as in [70]. In Eq. (19), any material tensor $\mathbf{a}$ is replaced by tensor $\left(\mathbf{R}\,\mathbf{a}\,\mathbf{R}^{\mathrm{T}}\right)$ then. In particular, for

Optics EXPRESS

normal incidence and propagation perpendicular to optical axis, material tensors are transformed to $\hat{\varepsilon}_{\mathrm{r}} = \mathrm{diag}\,[\varepsilon_{11}\ \varepsilon_{33}\ \varepsilon_{11}]$, $\hat{\alpha} = \mathrm{diag}\,[\alpha_{11}\ \alpha_{33}\ \alpha_{11}]$, and $\mathbf{N} = [0\ 0\ N_z]^{\mathrm{T}}$.

Substituting the particular forms of material tensors into (19), a following set of equations is obtained:

$$\begin{bmatrix} \varepsilon_{11} - N_z^2 - \alpha_{11}^2 & -i(\alpha_{11}+\alpha_{33})N_z & 0 \\ i(\alpha_{11}+\alpha_{33})N_z & \varepsilon_{33} - N_z^2 - \alpha_{33}^2 & 0 \\ 0 & 0 & \varepsilon_{11} - \alpha_{11}^2 \end{bmatrix} \begin{bmatrix} E_x \\ E_y \\ E_z \end{bmatrix} = 0. \tag{27}$$

Because the effect of $\hat{\alpha}$ is small [48,66], it is justifiable to set the term $(\hat{\alpha}\hat{\alpha}^{\mathrm{T}})$ in (19) to zero. Using (20), following set of equations is derived:

$$\begin{bmatrix} \varepsilon_{11} - N_z^2 & -ig_{11}N_z & 0 \\ ig_{11}N_z & \varepsilon_{33} - N_z^2 & 0 \\ 0 & 0 & \varepsilon_{11} \end{bmatrix} \begin{bmatrix} E_x \\ E_y \\ E_z \end{bmatrix} = 0. \tag{28}$$

By solving the equations that the determinants of (27) and (28) are equal to zero, normal eigenmodes $N_{z,k=\{1,2,3,4\}}$ propagating in bianisotropic nonmagnetic media of 32 point group perpendicular to optical axis are calculated, respectively, as follows:

$$N_{z,\alpha,k}^2 = \frac{\varepsilon_{11}+\varepsilon_{33}}{2} + \alpha_{11}\alpha_{33} \pm \sqrt{\left(\frac{\varepsilon_{11}-\varepsilon_{33}}{2}\right)^2 + (\alpha_{11}+\alpha_{33})(\varepsilon_{33}\alpha_{11}+\varepsilon_{11}\alpha_{33})}, \tag{29}$$

and

$$N_{z,g,k}^2 = \frac{\varepsilon_{11}+\varepsilon_{33}+g_{11}^2}{2} \pm \frac{\sqrt{g_{11}^4 + 2g_{11}^2 + (\varepsilon_{11}+\varepsilon_{33}) + (\varepsilon_{11}-\varepsilon_{33})^2}}{2}. \tag{30}$$

Both of the solutions stand for an elliptically polarized eigenmodes. For the case of small effect of the optical activity with respect to birefrigence, the eigenmodes with propagation constants (29) and (30) become linearly-like polarized and represent ordinary and extraordinary refractive indices of linear retarder $n_{\mathrm{o,e}}$,

$$N_{z,\alpha,(1,3)} \approx N_{z,g,(1,3)} \approx n_{\mathrm{o}}, \tag{31a}$$

$$N_{z,\alpha,(2,4)} \approx N_{z,g,(2,4)} \approx n_{\mathrm{e}}, \tag{31b}$$

and the optical activity influence comes from the ellipticity of the eigenmodes as the result of the intrinsicality of the OA. Moreover, by comparison of the wave Eq. (27) with (28) we find the symmetry between the formalism for this case [47,48],

$$g_{11} = \alpha_{11} + \alpha_{33}. \tag{32}$$

C. Mueller matrix of the chiral waveplate

Jones matrix describing a general elliptical retarder in the transmission configuration with retardation angle Γ is given as [26,71]

$$\mathbf{T} = \frac{1}{1+\chi\chi^*} \begin{bmatrix} \mathrm{e}^{i\frac{\Gamma}{2}} + \chi\chi^*\mathrm{e}^{-i\frac{\Gamma}{2}} & 2i\chi^* \sin\frac{\Gamma}{2} \\ 2i\chi \sin\frac{\Gamma}{2} & \chi\chi^*\mathrm{e}^{i\frac{\Gamma}{2}} + \mathrm{e}^{-i\frac{\Gamma}{2}} \end{bmatrix}, \tag{33}$$

where the complex ellipsometric parameter χ is related to the ellipticity ϵ of the polarization ellipse with its principal axes parallel to Cartesian coordinate system by

$$\chi = i\tan\epsilon \equiv i\kappa. \tag{34}$$

Optics EXPRESS

With this setting, Eq. (33) becomes [48,72]

$$\mathbf{T}_{\mathrm{R,EL}} = \frac{1}{1+\kappa^2}\begin{bmatrix} e^{i\frac{\Gamma}{2}} + \kappa^2 e^{-i\frac{\Gamma}{2}} & 2\kappa \sin\frac{\Gamma}{2} \\ -2\kappa \sin\frac{\Gamma}{2} & \kappa^2 e^{i\frac{\Gamma}{2}} + e^{-i\frac{\Gamma}{2}} \end{bmatrix}. \tag{35}$$

Corresponding transmission Mueller matrix of the elliptic retarder in a general azimuthal rotation φ is derived using

$$\mathbf{M}_{\mathrm{R,EL}}(\varphi,\,\Gamma,\,\kappa) = \mathbf{M}_{\varphi}^{\mathrm{T}} \underbrace{\mathbf{A}\left(\mathbf{T}_{\mathrm{R,EL}} \otimes \mathbf{T}_{\mathrm{R,EL}}^{*}\right)\mathbf{A}^{\mathrm{T}}}_{\mathbf{M}_{\mathrm{R,EL}}(\varphi=0,\,\Gamma,\,\kappa)} \mathbf{M}_{\varphi}, \tag{36}$$

where $\mathbf{M}_{\varphi}$ is the Mueller matrix of azimuthal rotation about the angle φ, the matrix $\mathbf{A}$ is the matrix relating the statistical properties of incident electric field to corresponding Stokes parameters [14], and the symbol $\otimes$ stands for the Kronecker product. Because the effect of the real parameter κ is small [48,66], it is justifiable to use Mueller matrix (36) linearly approximated in κ.

The resulting expression of the approximated matrix $\mathbf{M}_{\mathrm{R,EL}}(\varphi,\,\Gamma,\,\kappa)$ can be separated into two parts as

$$\mathbf{M}_{\mathrm{R,EL}}(\varphi,\,\Gamma,\,\kappa) = \mathbf{M}_{\mathrm{R,LIN}}(\varphi,\,\Gamma) + \mathbf{\Delta M}_{\mathrm{OA}}(\varphi,\,\Gamma,\,\kappa), \tag{37}$$

where

$$\mathbf{M}_{\mathrm{R,LIN}}(\varphi,\,\Gamma) = \begin{bmatrix} 1 & 0 & 0 & 0 \\ 0 & \cos^2 2\varphi + \cos\Gamma \sin^2 2\varphi & (1-\cos\Gamma)\sin 2\varphi \cos 2\varphi & -\sin 2\varphi \sin\Gamma \\ 0 & (1-\cos\Gamma)\sin 2\varphi \cos 2\varphi & \sin^2 2\varphi + \cos\Gamma \cos^2 2\varphi & \cos 2\varphi \sin\Gamma \\ 0 & \sin 2\varphi \sin\Gamma & -\cos 2\varphi \sin\Gamma & \cos\Gamma \end{bmatrix} \tag{38}$$

is the Mueller matrix for a non-gyrotropic linear retarder, and

$$\mathbf{\Delta M}_{\mathrm{OA}}(\varphi,\,\Gamma,\,\kappa) = \begin{bmatrix} 0 & 0 & 0 & 0 \\ 0 & 0 & 2\kappa \sin\Gamma & 4\kappa \cos 2\varphi \sin^2\frac{\Gamma}{2} \\ 0 & -2\kappa \sin\Gamma & 0 & 4\kappa \sin 2\varphi \sin^2\frac{\Gamma}{2} \\ 0 & 4\kappa \cos 2\varphi \sin^2\frac{\Gamma}{2} & 4\kappa \sin 2\varphi \sin^2\frac{\Gamma}{2} & 0 \end{bmatrix} \tag{39}$$

is the matrix (*not* a Mueller matrix [73]) describing the linear effect of the optical activity. Note, that the limit case of $\kappa = 0$ will turn the matrix $\mathbf{M}_{\mathrm{R,EL}}(\varphi,\,\Gamma,\,\kappa = 0)$ into the limit of standard linear retarder $\mathbf{M}_{\mathrm{R,LIN}}(\varphi,\,\Gamma)$. To show, that for $\kappa = 1$, Mueller matrix $\mathbf{M}_{\mathrm{R,EL}}(\varphi,\,\Gamma,\,\kappa = 1)$ corresponds to the Mueller matrix of circular retarder, a non-approximated matrix $\mathbf{M}_{\mathrm{R,EL}}(\varphi,\,\Gamma,\,\kappa)$ in the form of 36 regarding strong effects of κ must be used.

The gyration parameter κ is usually derived [45,47,48,57] from the eigenvalue problem of the wave equation based on the Born-Landau constitution relations. The resultant expression with respect to the linear approximation of κ is given as

$$\kappa = \frac{1}{2G}\left[\left(n_{\mathrm{e}}^2 - n_{\mathrm{o}}^2\right) - \sqrt{\left(n_{\mathrm{e}}^2 - n_{\mathrm{o}}^2\right)^2 + 4G^2}\right], \tag{40}$$

where $n_{\mathrm{o}} = \sqrt{\varepsilon_{11}}$, $n_{\mathrm{e}} = \sqrt{\varepsilon_{33}}$ are ordinary and extraordinary refractive indices (without the effect of optical activity) of the uniaxial medium, respectively.

Optics EXPRESS

For point group 32, scalar gyration parameter G [Eq. (23)] is given by the non-zero components of $\hat{g}$ and the angle θ given by (24),

$$G = g_{11}\sin^2\theta + g_{33}\cos^2\theta. \tag{41}$$

The dispersion characteristics of the components of gyration tensor $\hat{g}$ were derived in [47] and are given by the dispersion equation

$$g_{ii} = \frac{A_i\lambda^3}{\left(\lambda^2 - B_i^2\right)^2}, \quad i = \{1, 3\}, \tag{42}$$

where λ is the wavelength and A_i, B_i are phenomenological constants. This dispersion model is based on the sum rule consistent model of coupled anisotropic oscillators, and was originally developed for the description of specific rotatory power dispersion [74].

D. Algebraic analysis of the optical activity and misalignment effects in the Mueller matrix of biplates

Let us consider the Mueller matrix of biplate in the form of (7), which differs from an ideal biplate by the presence of the waveplate misalignment $\Phi = \varphi_1 - \varphi_2 - \pi/2$ and the OA $\mathbf{M}_{\mathrm{R,EL}}(\varphi,\ \Gamma_1 - \Gamma_2, \kappa)$ given by (5), introduced as follows:

$$\mathbf{M}_{\mathrm{R,WB}} = \mathbf{M}_{\mathrm{R,EL2}}\left(\varphi + \frac{\Phi}{2} + \frac{\pi}{2},\ \Gamma_2,\ \kappa\right)\mathbf{M}_{\mathrm{R,EL1}}\left(\varphi - \frac{\Phi}{2},\ \Gamma_1,\ \kappa\right). \tag{43}$$

Considering only small effects in both misalignment and OA (κ, $\Phi \ll 1$), we express Mueller matrix (43) as its first order Taylor expansions. The resulting form of the matrix $\mathbf{M}_{\mathrm{R,WB}}$ is then represented as a sum of the Mueller matrix of an ideal biplate without the OA and perturbation matrices, each representing separate contribution of the OA and the misalignment in the form of fine spectral oscillations:

$$\mathbf{M}_{\mathrm{R,WB}} \approx \mathbf{M}_{\mathrm{R,LIN}}(\varphi,\ \Delta\Gamma) + \begin{bmatrix} 1 & \mathbf{0}^{\mathrm{T}} \\ \mathbf{0} & \mathbf{m}_\kappa \end{bmatrix} + \begin{bmatrix} 1 & \mathbf{0}^{\mathrm{T}} \\ \mathbf{0} & \mathbf{m}_\Phi \end{bmatrix}, \tag{44}$$

where

$$\mathbf{m}_\Phi = \Phi\begin{bmatrix} -\mathrm{S}_{4\varphi}(\mathrm{C}_{\Gamma_1} - \mathrm{C}_{\Gamma_2}) & \mathrm{C}_{4\varphi}(\mathrm{C}_{\Gamma_1} - \mathrm{C}_{\Gamma_2}) + W & \mathrm{C}_{2\varphi}(2\mathrm{S}_{\Gamma_1} - \mathrm{S}_{\Delta\Gamma}) \\ \mathrm{C}_{4\varphi}(\mathrm{C}_{\Gamma_1} - \mathrm{C}_{\Gamma_2}) - W & \mathrm{S}_{4\varphi}(\mathrm{C}_{\Gamma_1} - \mathrm{C}_{\Gamma_2}) & \mathrm{S}_{2\varphi}(2\mathrm{S}_{\Gamma_1} - \mathrm{S}_{\Delta\Gamma}) \\ -\mathrm{C}_{2\varphi}(2\mathrm{S}_{\Gamma_2} + \mathrm{S}_{\Delta\Gamma}) & -\mathrm{S}_{2\varphi}(2\mathrm{S}_{\Gamma_2} + \mathrm{S}_{\Delta\Gamma}) & 0 \end{bmatrix}, \tag{45}$$

$$\mathbf{m}_\kappa = \kappa\begin{bmatrix} 2\mathrm{S}_{4\varphi}V & 2\mathrm{S}_{\Gamma_1} + 2\mathrm{S}_{\Gamma_2} - 2\mathrm{C}_{4\varphi}V & 2\mathrm{C}_{2\varphi}(\mathrm{C}_{\Delta\Gamma} - 2\mathrm{C}_{\Gamma_1} + 1) \\ -2\mathrm{S}_{\Gamma_1} - 2\mathrm{S}_{\Gamma_2} - 2\mathrm{C}_{4\varphi}V & -2\mathrm{S}_{4\varphi}V & 2\mathrm{S}_{2\varphi}(\mathrm{C}_{\Delta\Gamma} - 2\mathrm{C}_{\Gamma_1} + 1) \\ -2\mathrm{C}_{2\varphi}(\mathrm{C}_{\Delta\Gamma} - 2\mathrm{C}_{\Gamma_2} + 1) & -2\mathrm{S}_{2\varphi}(\mathrm{C}_{\Delta\Gamma} - 2\mathrm{C}_{\Gamma_2} + 1) & 0 \end{bmatrix}, \tag{46}$$

and

$$\Delta\Gamma = \Gamma_1 - \Gamma_2, \tag{47a}$$

$$\mathrm{S}_{\mathrm{arg}} = \sin(\mathrm{arg}), \qquad \mathrm{C}_{\mathrm{arg}} = \cos(\mathrm{arg}), \tag{47b}$$

$$V = \mathrm{S}_{\Gamma_2} - \mathrm{S}_{\Gamma_1} + \mathrm{S}_{\Delta\Gamma}, \qquad W = \mathrm{C}_{\Gamma_1} + \mathrm{C}_{\Gamma_2} - \mathrm{C}_{\Delta\Gamma} - 1. \tag{47c}$$

Optics EXPRESS

Funding. Grantová Agentura České Republiky (18-22102S); European Regional Development Fund (CZ.02.1.01/0.0/0.0/16_013/0001791); EEA and Norway grants (EMP-CZ-MOP-2-013); Technology Agency of the Czech Republic (FV20020); DGS - Doctoral Grant System (CZ.02.2.69/0.0./0.0/19_073/0016945, Project DGS/TEAM/2020-030); SGS - Student Grant System (SP2020/71).

Acknowledgment. Partial support from the Czech Science Foundation (Project 18-22102S), the IT4Innovations Path to Exascale project CZ02.1.01/0.0/0.0/16013/0001791, EEA grant (EMP-CZ-MOP-2-013), the Project FV20020, doctoral grant system (CZ.02.2.69/0.0./0.0/19_073/0016945, Project DGS/TEAM/2020-030), and student grant system (SP2020/71) are acknowledged.

Disclosures. The authors declare no conflicts of interest.

References

1. M. Haiml, R. Grange, and U. Keller, "Optical characterization of semiconductor saturable absorbers," Appl. Phys. B **79**(3), 331–339 (2004).
2. D. J. Dixit, S. O'Mullane, S. Sunkoju, A. Gottipati, E. R. Hosler, V. K. Kamineni, M. E. Preil, N. Keller, J. Race, G. R. Muthinti, and A. C. Diebold, "Sensitivity analysis and line edge roughness determination of 28-nm pitch silicon fins using Mueller matrix spectroscopic ellipsometry-based optical critical dimension metrology," J. Micro/Nanolith. MEMS MOEMS **14**(3), 031208 (2015).
3. H.-T. Huang and F. L. Terry Jr., "Spectroscopic ellipsometry and reflectometry from gratings (Scatterometry) for critical dimension measurement and in situ, real-time process monitoring," Thin Solid Films **455-456**, 828–836 (2004).
4. M. Foldyna, T. Germer, and B. Bergner, "Mueller matrix ellipsometry of artificial non-periodic line edge roughness in presence of finite numerical aperture," Proc. SPIE **7971**, 79710N (2011).
5. J.-B. Masson and G. Gallot, "Terahertz achromatic quarter-wave plate," Opt. Lett. **31**(2), 265–267 (2006).
6. D. Wang, L. Zhang, Y. Gu, M. Q. Mehmood, Y. Gong, A. Srivastava, L. Jian, T. Venkatesan, C.-W. Qiu, and M. Hong, "Switchable Ultrathin Quarter-wave Plate in Terahertz Using Active Phase-change Metasurface," Sci. Rep. **5**(1), 15020 (2015).
7. D. Vala, M. Mčica, K. Postava, and J. Pištora, "Optical activity temperature-dependent measurements of chiral solutions using Mueller matrix spectroscopic ellipsometry," Proc. SPIE **10976**, 109760A (2018).
8. H. Lundén, A. Liotta, D. Chateau, F. Lerouge, F. Chaput, S. Parola, C. Brännlund, Z. Ghadyani, M. Kildemo, M. Lindgren, and C. Lopes, "Dispersion and self-orientation of gold nanoparticles in sol-gel hybrid silica – optical transmission properties," J. Mater. Chem. C **3**(5), 1026–1034 (2015).
9. Q.-H. Phan and Y.-L. Lo, "Stokes-Mueller matrix polarimetry system for glucose sensing," Opt. Lasers Eng. **92**, 120–128 (2017).
10. R. M. A. Azzam, "Mueller-matrix ellipsometry: A review," in *Polarization: Measurement, Analysis, and Remote Sensing*, vol. 3121 (International Society for Optics and Photonics, 1997), pp. 396–405.
11. K. Postava, R. Sýkora, D. Legut, and J. Pištora, "Determination of Anisotropic Crystal Optical Properties Using Mueller Matrix Spectroscopic Ellipsometry," Procedia Mater. Sci. **12**, 118–123 (2016).
12. M. Kildemo, J.-P. Banon, A. Baron, B. B. Svendsen, T. Brakstad, and I. Simonsen, "Optical response of gold hemispheroidal lattices on transparent substrates," Appl. Surf. Sci. **421**, 593–600 (2017).
13. K. Postava, A. Maziewski, T. Yamaguchi, R. Ossikovski, Š. Višňovský, and J. Pištora, "Null ellipsometer with phase modulation," Opt. Express **12**(24), 6040–6045 (2004).
14. E. Garcia-Caurel, R. Ossikovski, M. Foldyna, A. Pierangelo, B. Drévillon, and A. De Martino, "Advanced Mueller Ellipsometry Instrumentation and Data Analysis," in *Ellipsometry at the Nanoscale*, (Springer, 2013), pp. 31–143.
15. V. Andreev, C. Panda, P. Hess, B. Spaun, and G. Gabrielse, "A self-calibrating polarimeter to measure Stokes parameters.," ResearchGate (2017).
16. F. Stabo-Eeg, "Development of instrumentation for Mueller matrix ellipsometry," Ph.D. thesis, Norwegian University of Science and Technology (2009).
17. A. Pierangelo, A. Benali, M.-R. Antonelli, T. Novikova, P. Validire, B. Gayet, and A. De Martino, "Ex-vivo characterization of human colon cancer by Mueller polarimetric imaging," Opt. Express **19**(2), 1582–1593 (2011).
18. P. A. Letnes, I. S. Nerbø, L. M. S. Aas, P. G. Ellingsen, and M. Kildemo, "Fast and optimal broad-band Stokes/Mueller polarimeter design by the use of a genetic algorithm," Opt. Express **18**(22), 23095–23103 (2010).
19. T. Golovina, A. Konstantinova, B. Nabatov, and E. Evdishchenko, "Determination of the Optical Parameters of Uniaxial Optically Active Crystals Taking into Account the Imperfection of Spectrophotometric Complex Elements," Crystallogr. Rep. **63**(6), 964–968 (2018).
20. A. F. Konstantinova, T. G. Golovina, E. A. Evdishchenko, B. V. Nabatov, and G. I. Utkin, "Determination of the Optical Parameters of Uniaxial Crystals with Allowance for the Imperfection of the Spectrophotometric Complex Elements," Crystallogr. Rep. **63**(4), 606–613 (2018).
21. J. S. Jackson, J. L. Archibald, and D. S. Durfee, "Light splitting with imperfect wave plates," Appl. Opt. **56**(4), 1062–1068 (2017).
22. B. Boulbry, B. Bousquet, B. L. Jeune, Y. Guern, and J. Lotrian, "Polarization errors associated with zero-order achromatic quarter-wave plates in the whole visible spectral range," Opt. Express **9**(5), 225–235 (2001).

Optics EXPRESS

23. L. Broch, A. E. Naciri, and L. Johann, "Systematic errors for a Mueller matrix dual rotating compensator ellipsometer," Opt. Express **16**(12), 8814–8824 (2008).
24. E. A. West and M. H. Smith, "Polarization errors associated with birefringent waveplates," Opt. Eng. **34**(6), 1574–1580 (1995).
25. D. Bergman, "Analysis of elliptically polarized light," J. Opt. Soc. Am. **52**(9), 1080 (1962).
26. R. M. A. Azzam and N. M. Bashara, *Ellipsometry and Polarized Light* (North-Holland Publishing Company, 1977).
27. H. Fujiwara, *Spectroscopic Ellipsometry: Principles and Applications* (Wiley, 2007).
28. J. M. Beckers, "Achromatic linear retarders," Appl. Opt. **10**(4), 973–975 (1971).
29. P. Koleják, D. Vala, K. Postava, P. Provazníková, and J. Pištora, "Mueller matrix ellipsometry of waveplates for control of their properties and alignment," J. Vac. Sci. Technol., B: Nanotechnol. Microelectron.: Mater., Process., Meas., Phenom. **38**(1), 014006 (2020).
30. T. Novikova, J. Rehbinder, S. Deby, H. Haddad, J. Vizet, A. Pierangelo, P. Validire, A. Benali, B. Gayet, B. Teig, A. Nazac, B. Drévillon, F. Moreau, and A. D. Martino, "Multi-spectral mueller matrix imaging polarimetry for studies of human tissues," in *Biomedical Optics 2016*, (Optical Society of America, 2016), p. TTh3B.2.
31. L. Halagačka, K. Postava, and J. Pištora, "Analysis and Modeling of Depolarization Effects in Mueller Matrix Spectroscopic Ellipsometry Data," Procedia Mater. Sci. **12**, 112–117 (2016).
32. M. Foldyna, A. De Martino, R. Ossikovski, E. Garcia-Caurel, and C. Licitra, "Characterization of grating structures by Mueller polarimetry in presence of strong depolarization due to finite spot size," Opt. Commun. **282**(5), 735–741 (2009).
33. D. E. Aspnes, "Expanding horizons: New developments in ellipsometry and polarimetry," Thin Solid Films **455-456**, 3–13 (2004).
34. B. Johs and C. M. Herzinger, "Quantifying the accuracy of ellipsometer systems," Phys. Status Solidi C **5**(5), 1031–1035 (2008).
35. S.-Y. Lu and R. A. Chipman, "Interpretation of Mueller matrices based on polar decomposition," J. Opt. Soc. Am. A **13**(5), 1106–1113 (1996).
36. H. Gu, S. Liu, X. Chen, and C. Zhang, "Calibration of misalignment errors in composite waveplates using Mueller matrix ellipsometry," Appl. Opt. **54**(4), 684–693 (2015).
37. H. Gu, X. Chen, Y. Shi, H. Jiang, C. Zhang, P. Gong, and S. Liu, "Comprehensive characterization of a general composite waveplate by spectroscopic Mueller matrix polarimetry," Opt. Express **26**(19), 25408–25425 (2018).
38. F. I. Fedorov, *Theory of gyrotropy [in russian]* (Nauka i Technika, 1964).
39. F. I. Fedorov, *Optics of anisotropic media [in russian]* (Izdatělstvo Naučnoj i Učebnoj Literatury, 2004).
40. A. Yariv and P. Yeh, *Optical Waves in Crystals: Propagation and Control of Laser Radiation* (Wiley, 2002).
41. E. U. Condon, "Theories of Optical Rotatory Power," Rev. Mod. Phys. **9**(4), 432–457 (1937).
42. M. De Graef and M. E. McHenry, *Structure of Materials: An Introduction to Crystallography, Diffraction and Symmetry* (Cambridge University Press, 2012), 2nd ed.
43. D. E. Sands, *Introduction to Crystallography* (Courier Corporation, 1993).
44. D. Franta, "Symmetry of linear dielectric response tensors: Dispersion models fulfilling three fundamental conditions," J. Appl. Phys. **127**(22), 223101 (2020).
45. J. F. Nye, *Physical Properties of Crystals: Their Representation by Tensors and Matrices* (Clarendon, 1985).
46. F. G. Fumi, "Physical properties of crystals: The direct-inspection method," Acta Crystallogr. **5**(1), 44–48 (1952).
47. O. Arteaga, A. Canillas, and G. Jellison, "Determination of the components of the gyration tensor of quartz by oblique incidence transmission two-modulator generalized ellipsometry," Appl. Opt. **48**(28), 5307–5317 (2009).
48. A. F. Konstantinova, B. N. Grečušnikov, B. V. Bokut', and E. G. Valjaško, *Optical properties of crystals [in russian]* (Nauka i Technika, 1995).
49. O. Arteaga and A. Canillas, "Pseudopolar decomposition of the jones and mueller-jones exponential polarization matrices," J. Opt. Soc. Am. A **26**(4), 783–793 (2009).
50. J. Cervantes-L, D. I. Serrano-Garcia, Y. Otani, and B. Cense, "Mueller-matrix modeling and characterization of a dual-crystal electro-optic modulator," Opt. Express **24**(21), 24213–24224 (2016).
51. D. Kliger and J. Lewis, *Polarized Light in Optics and Spectroscopy* (Academic, 2012).
52. S.-M. F. Nee, "Depolarization and retardation of a birefringent slab," J. Opt. Soc. Am. A **17**(11), 2067–2073 (2000).
53. T. A. Germer and H. J. Patrick, "Effect of bandwidth and numerical aperture in optical scatterometry," in *Metrology, Inspection, and Process Control for Microlithography XXIV*, vol. 7638 (International Society for Optics and Photonics, 2010), p. 76381F.
54. T. Radhakrishnan, "Further studies on the temperature variation of the refractive index of crystals," Proc. - Indian Acad. Sci., Sect. A **33**(1), 22–34 (1951).
55. T. Radhakrishnan, "The dispersion, briefringence and optical activity of quartz," Proc. - Indian Acad. Sci., Sect. A **25**(3), 260–265 (1947).
56. I. V. Lindell, A. H. Sihvola, A. J. Viitanen, and S. A. Tretyakov, *Electromagnetic Waves in Chiral and Bi-isotropic Media* (Artech House, 1994).
57. A. F. Konstantinova, B. V. Nabatov, E. A. Evdishchenko, and K. K. Konstantinov, "Modern application packages for rigorous solution of problems of light propagation in anisotropic layered media: II. Optically active crystals," Crystallogr. Rep. **47**(5), 815–823 (2002).

Optics EXPRESS

58. A. H. Sihvola and I. V. Lindell, "Bi-isotropic constitutive relations," Microw. Opt. Technol. Lett. **4**(8), 295–297 (1991).
59. B. D. H. Tellegen, "The Gyrator: A New Electric Network Element," Philips Res. Rept. **3**, 81–101 (1985).
60. S. A. Tretyakov, A. H. Sihvola, A. A. Sochava, and C. R. Simovski, "Magnetoelectric Interactions in Bi-Anisotropic Media," J. Electromagn. Waves Appl. **12**(4), 481–497 (1998).
61. L. Onsager, "Reciprocal Relations in Irreversible Processes. I.," Phys. Rev. **37**(4), 405–426 (1931).
62. L. Onsager, "Reciprocal Relations in Irreversible Processes. II.," Phys. Rev. **38**(12), 2265–2279 (1931).
63. H. Casimir, "On Onsager's Principle of Microscopic Reversibility," Rev. Mod. Phys. **17**(2-3), 343–350 (1945).
64. S. Tretyakov, A. Sihvola, and B. Jancewicz, "Onsager-Casimir Principle and the Constitutive Relations of Bi-Anisotropic Media," J. Electromagn. Waves Appl. **16**(4), 573–587 (2002).
65. L. M. Barkovsky and G. N. Borzdov, "V.A. Shamburov's validity criteria for the gyrotropy theory," Opt. Spectrosc. **95**(1), 124–130 (2003).
66. R. Ossikovski and O. Arteaga, "Extended Yeh's method for optically active anisotropic layered media," Opt. Lett. **42**(18), 3690–3693 (2017).
67. K. Postava, J. Pištora, and P. Hlubina, "Effect of permeability on guided modes in planar structures," Proc. SPIE **3573**, 524–527 (1998).
68. L. D. Landau, L. P. Pitaevskii, and E. M. Lifshitz, *Electrodynamics of Continuous Media: Volume 8 (Course of Theoretical Physics S)* (Butterworth-Heinemann, 1984).
69. D. Franta and J. Vohánka, "Constitutive equations describing optical activity in theory of dispersion," J. Opt. Soc. Am. B **38**(2), 553–561 (2021).
70. H. Goldstein, C. P. Poole Jr., and J. L. Safko, *Classical Mechanics* (3rd Edition) (Pearson, 2001).
71. J. J. Gil Perez and R. Ossikovski, *Polarized Light and the Mueller Matrix Approach* (Taylor & Francis, 2017).
72. E. A. Evdischenko and A. F. Konstantinova, *Jones Transmission and Reflection Matrices for Low-Symmetric Absorbing Gyrotropic Crystals* (Springer, 1997), pp. 67–70.
73. D. G. M. Anderson and R. Barakat, "Necessary and sufficient conditions for a Mueller matrix to be derivable from a Jones matrix," J. Opt. Soc. Am. A **11**(8), 2305–2319 (1994).
74. C. Sivaramakrishna and B. W. Lawrence, "Optical rotatory dispersion of crystals," Proc. R. Soc. London A – Math. Phys. Sci. **259**, 531–553 (1961).